PHYSICAL REVIEW B **86**, 064408 (2012)

Multiferroicity in geometrically frustrated α-MCr_2O_4 systems (M = Ca, Sr, Ba)

Li. Zhao, Tian-Wey Lan, Kuen-Jen Wang, Chia-Hua Chien, Tsu-Lien Hung, Jiu-Yong Luo, Wei-Hsiang Chao, Chung-Chieh Chang, Yang-Yuan Chen, and Maw-Kuen Wu*
Institute of Physics, Academia Sinica, Taipei 11529, Taiwan

Christine Martin
Laboratoire CRISMAT, ENSICAEN, UMR 6508 CNRS, 6 Boulevard du Marchal Juin, 14050 Caen Cedex, France
(Received 27 May 2012; published 3 August 2012)

We have successfully synthesized three quasi-two-dimensional geometrically frustrated magnetic compounds (α-MCr_2O_4, M = Ca, Sr, Ba) using the spark-plasma-sintering technique. All these members of the α-MCr_2O_4 family consist of the stacking planar triangular lattices of Cr^{3+} spins ($S = 3/2$), separated by nonmagnetic alkaline-earth ions. Their corresponding magnetic susceptibility, specific heat, dielectric permittivity, and ferroelectric polarization are systematically investigated. A long-range magnetic ordering arises below the Néel temperature (around 40 K) in each member of the α-MCr_2O_4 family, which changes to the quasi-120° proper-screw-type helical spin structure at low temperature. A very small but confirmed spontaneous electric polarization emerges concomitantly with this magnetic ordering. The direction of electric polarization is found within the basal triangular plane. The multiferroicity in α-MCr_2O_4 can not be explained within the frameworks of the magnetic exchange striction or the inverse Dzyaloshinskii-Moriya interaction. The observed results are more compatible with the newly proposed Arima mechanism that is associated with the d-p hybridization between the ligand and transition-metal ions, modified by the spin-orbit coupling. The evolution of multiferroic properties with the increasing interplanar spacing (as M changes from Ca to Ba) reveals the importance of interlayer interaction in this new family of frustrated magnetic systems.

DOI: 10.1103/PhysRevB.86.064408 PACS number(s): 75.85.+t, 75.10.Jm, 77.22.−d, 77.80.−e

I. INTRODUCTION

Multiferroics, also known as "magnetic ferroelectrics," which exhibit the coexisting and mutual interaction of magnetism and ferroelectricity in one single phase, have been one of the most important topics that attract worldwide interest form the condensed matter physics and material science research communities. The recent discovery of giant magnetoelectric coupling effect in some frustrated manganites such as $TbMnO_3$ and $TbMn_2O_5$ that exhibit multiferroicity has further enhanced the interest.[1,2] The ferroelectricity found in these frustrated manganites is of magnetic origin, i.e., induced by complex spin orderings. These systems are thus often called "spin-driven ferroelectrics," as their spontaneous electric polarization arises in certain magnetically ordered states that break the inversion symmetry. The electric polarization can be reversed or even rotated by changing the magnetic states via the application of external magnetic fields. These fascinating phenomena are of great importance for both fundamental physics and potential technological application.[3–6]

The physical origin of multiferroicity is still a matter of debate. Although at present there is no commonly accepted unified microscopic theory, several possible mechanisms have been proposed to provide the understanding of some certain multiferroic systems.[6] One simple mechanism for multiferroicity is the exchange striction in certain (quasi)collinear commensurate spin configurations with inequivalent magnetic ions.[4,6] For example, the inequivalent nearest-neighbor exchange striction in a one-dimensional (1D) collinear ↑↑↓↓ spin chain system can break the space inversion via shifting ions away from centrosymmetric positions, then induce a spontaneous electric polarization along the spin chain, as observed in Ca_3(Co, Mn)O_6.[7] But, the spin configurations in most of the known multiferroic materials are much more complex at low temperatures, which are usually noncollinear and incommensurate. Thus, alternative mechanisms were proposed for the noncollinear spin ordering.

According to the inverse Dzyaloshinskii-Moriya (DM) mechanism[8] or the equivalent spin-current model (proposed by Katsura, Nagaosa, and Balatsky, also known as the KNB model),[9] the two neighboring atomic sites with mutually canted spins will induced a local electric polarization via spin-orbit interaction. This induced local polarization can be formulated as $\boldsymbol{P}_{ij} = A\hat{\mathbf{e}}_{ij} \times (\boldsymbol{S}_i \times \boldsymbol{S}_j)$, where the coupling coefficient A is determined by the spin-orbit coupling and exchange interactions. $\hat{\mathbf{e}}_{ij}$ is the unit vector connecting sites i and j. This expression is also consistent with the phenomenological theory based on symmetry consideration,[10] and has explained qualitatively the origin of the ferroelectricity in several helical magnetic systems such as $TbMnO_3$,[8] $LiCu_2O_2$,[11] etc.

Nevertheless, it is noted that the above mechanisms can not predict any electric polarization for a class of so-called "proper-screw-type" helimagnets, in which the magnetic modulation vector is parallel to the spin helicity (defined as $\boldsymbol{S}_i \times \boldsymbol{S}_j$). However, multiferroicity has been discovered in several delafossitelike magnetic materials with hexagonal lattices, such as $CuFeO_2$,[12] $ACrO_2$ (A = Cu, Ag),[13] etc. These materials are all low-dimensional triangular-lattice antiferromagnets with strong geometrical magnetic frustration. The corresponding spontaneous electric polarization arises concurrently with the emerging proper-screw magnetic ordering at low temperature. To account for these experimental observations, Arima[14] and Jia *et al.*[15] proposed a new theoretical scheme recently in which the certain types

of proper-screw spin orderings are capable of inducing macroscopic electric polarization through the variation in the metal-ligand hybridization with spin-orbit coupling. However, until now, a unified understanding and quantitative prediction of multiferroicity still lacks in the present research.

On the other hand, the research of the geometrically magnetic frustration in the strongly correlated electronic systems long has been of interest.[16] Usually, the short-range orderings, strong fluctuations, rich phase diagrams, and novel critical phenomena arise at low temperatures in these systems, providing a fertile ground for physicists. The competing neighboring magnetic interactions lead to the extra degeneracy in ground state over and above the nonfrustrated systems, which give rise to the emerging of new physics. The anisotropy of magnetic ions (of easy-axis or easy-plane type), the interlayer coupling, etc., also play important roles in real systems. The simplest form of the magnetically geometrical frustration can arise from a two-dimensional (2D) triangular arrangement of magnetic ions that are coupled antiferromagnetically with each other. Theoretically, for an ideal 2D triangular lattice of identical classical vector spins, there are degenerate solutions for the lowest energy of the system in which each given spin vector is arranged at 120° to its nearest neighbors. The highly degenerate ground states lead to exotic physical magnetic behaviors, such as short-range ordered spin-liquid states, or long-range chiral magnetic orderings.[17] In real antiferromagnets with quasi-2D triangular lattice, the intralayer structural distortions from an ideal regular triangular lattice, the interlayer magnetic exchange interactions, and the anisotropy of magnetic ions can act as important additional terms, leading to many different types of magnetic structures. For example, the interlayer interactions can stabilize the long-range magnetic ordering at higher temperatures, and the strong single-ion anisotropy favors the collinear ordering in the ground state. There are still many open questions about the physical behavior of geometrically frustrated magnets.

In this paper, we investigate the α-phase $M\mathrm{Cr_2O_4}$ family systematically, where M stands for different alkaline-earth metal (M = Ca, Sr, or Ba). As shown in Fig. 1, the α-phase $M\mathrm{Cr_2O_4}$ has a quasi-2D layered structure with triangular $\mathrm{CrO_2}$ sheets, which are made of edge-sharing $\mathrm{CrO_6}$ octahedra. These stacking $\mathrm{CrO_2}$ sheets are well separated by nonmagnetic ions of alkaline-earth metal. The different M atoms primarily manifest in different separation (d) between the triangular $\mathrm{CrO_2}$ sheets. With increasing cationic radius, d increases markedly, i.e., d = 5.53, 5.82, and 6.14 Å for M = Ca, Sr, and Ba, respectively.

In each $\mathrm{CrO_2}$ layer, the neighboring $\mathrm{Cr^{3+}}$-$\mathrm{Cr^{3+}}$ distance is short (close to 3 Å), resulting in a strong direct antiferromagnetic exchange interaction, while the intralayer superexchange is known to be quite weak since the $\mathrm{Cr^{3+}}$-O-$\mathrm{Cr^{3+}}$ bonding angle is around 95°.[18] The exchange interaction between interlayer $\mathrm{Cr^{3+}}$ ions is quite weak due to much larger distance between layers. The structure of α-$M\mathrm{Cr_2O_4}$ resembles the hexagonal delafossites closely, with a slight rectangular distortion in the $\mathrm{CrO_2}$ layers from the ideal regular triangular lattice. This kind of distortion results an overall orthorhombic symmetry in α-$M\mathrm{Cr_2O_4}$ with two inequivalent $\mathrm{Cr^{3+}}$ sites as shown in Fig. 1(b).

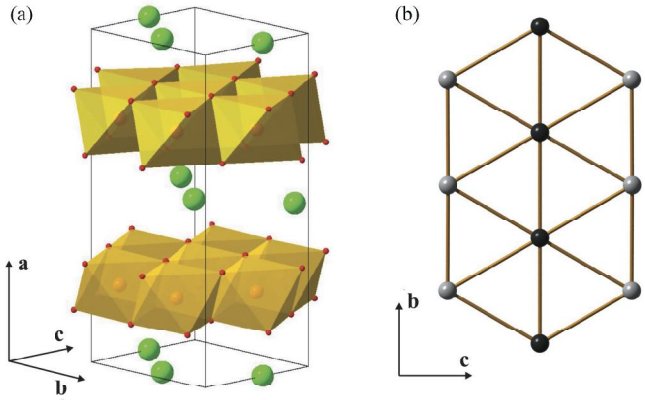

FIG. 1. (Color online) (a) Crystal structure of α-$M\mathrm{Cr_2O_4}$. The large green spheres stand for the alkaline-earth ions (M = Ca, Sr, Ba). The small red balls represent the oxygen ions, forming the octahedra in which there are chromium cations. (b) Projection along the a axis of a single triangular $\mathrm{CrO_2}$ layer with only the $\mathrm{Cr^{3+}}$ network. Two kinds of the inequivalent $\mathrm{Cr^{3+}}$ sites are plotted as the dark and light gray spheres, respectively.

Although α-phase $M\mathrm{Cr_2O_4}$ had been synthesized and structurally characterized dozens of years ago,[19–21] their physical properties at low temperature have not been investigated until recently. Chapon *et al.*[22] first investigated the magnetism and magnetic structure of polycrystalline α-$\mathrm{CaCr_2O_4}$. A long-range ordered helical magnetic structure in α-$\mathrm{CaCr_2O_4}$ occurs below the Néel temperature (T_N) of about 43 K with an incommensurate propagation vector $\mathbf{k} = (\mathbf{0}, \sim 1/3, 0)$. The neutron diffraction experiment revealed that the spins in $\mathrm{CrO_2}$ layer lie in the ac plane, perpendicular to the $\mathbf{k}$ vector. This is a typical "proper-screw-type" helimagnetic structure. In addition, the angle between the neighboring spins is around 120°, which is very close to the theoretical expected value for an ideal 2D triangular antiferromagnetic lattice, in spite of the orthorhombic distortion in α-$\mathrm{CaCr_2O_4}$. Later, a neutron measurement on crystal samples further confirmed this quasi-120° helical spin picture.[23]

In 2011, Cava's group[24] synthesized the polycrystalline α-$\mathrm{SrCr_2O_4}$, a Sr version of α-$M\mathrm{Cr_2O_4}$ with an expanded spacing between the $\mathrm{CrO_2}$ layers and also a slightly larger intralayer orthogonal distortion. The powder neutron diffraction measurements show a very similar incommensurate helical spin ordering arising below almost the same magnetic transition temperature as in α-$\mathrm{CaCr_2O_4}$. Replacing $\mathrm{Ca^{2+}}$ ions with larger $\mathrm{Sr^{2+}}$ ones seemed incapable of bringing about significant changes in the physical properties in this class of materials. Further measurements on the temperature-dependent structure parameters revealed an anomalous slight inflection in the lattice parameter perpendicular to $\mathrm{CrO_2}$ layers around T_N, suggesting a possible magnetostructural coupling. The quadratic magnetoelectric effect was also predicted based on a Landau symmetry analysis. Recently, the neutron diffraction measurements on bulk samples of α-$\mathrm{BaCr_2O_4}$ by Hardy *et al.* disclosed a similar long-range incommensurate helimagnetic phase below T_N, very close to the above quasi-120° spin structure, which will be discussed elsewhere.[25]

In addition, Singh *et al.*[26] reported the multiferroicity existing in the bulk samples of α-$\mathrm{CaCr_2O_4}$. The weak

ferroelectricity occurs concomitantly with the incommensurate helical magnetic ordering below T_N of α-$CaCr_2O_4$. But, no further microscopic mechanism is given. Based on the structural similarity, we can reasonably expect that the similar multiferroicity also exists in the other two analogs in the α-MCr_2O_4 family. Therefore, the systematical study on this family is clearly needed to clarify their microscopic physical origin of the multiferroicity and search for new promising multiferroic materials among the geometrically frustrated triangular systems.

Herein, we report the study of all the three member compounds (M = Ca, Sr, and Ba) using samples of high quality. Based on the measurements of the magnetic susceptibility, specific heat, and, especially, dielectric and ferroelectric properties, our work confirms the spin-driven ferroelectricity in this family. In the following, we first focus on α-$SrCr_2O_4$ (the middle member in this family) and then systematically compare it with the other two members (α-phase $CaCr_2O_4$ and $BaCr_2O_4$). We also provide our view on the possible physical mechanisms for the observed multiferroicity.

II. EXPERIMENTAL DETAILS

Our polycrystalline samples of α-MCr_2O_4 (M = Ca, Sr, Ba) were prepared by the spark-plasma-sintering (SPS) method. All these compounds own very high melting points (T_{mp}). For M = Ca and Sr, $T_{mp} > 2000\,^{\circ}$C. As for Ba, $T_{mp} > 1600\,^{\circ}$C.[19–21] A rather high sintering temperature ($>1400\,^{\circ}$C) is necessary to prepare pure α-phase samples because of a two-phase competition in the MCr_2O_4 system. The α-phase MCr_2O_4 favors high sintering temperature, while another β phase is prone to appear in low temperature.[27] A controlled atmosphere is also necessary to prevent low-valence Cr^{3+} ions from being further oxidized. Compared with the conventional solid-state sintering synthesis, the new powerful SPS technique can be used to prepare many refractory materials productively with high density and it also facilitates a very high heating and cooling rate to avoid β phase as impurity in our samples (a rate of about $200\,^{\circ}$C/min is adopted in our experiments).

The starting materials of MCr_2O_4 for SPS processing are prepared by a conventional ceramic synthesis route. The stoichiometric mixture of Cr_2O_3 and MCO_3 with high purity was sintered at $1050\,^{\circ}$C under a dynamic high vacuum (below 10^{-6} Torr) for 72 h with several intermediate grindings. Then, the precursor was loaded into a graphite die, consolidated by SPS processing. The sample is kept at $1400\,^{\circ}$C–$1500\,^{\circ}$C for at least 20 min under a uniaxial pressure of 40 MPa and a very large dc current (over 1000 A) is applied, using a Dr. Sinter 1500 SPS machine (SPS SYNTEX Inc.). The final products are very dense pellets with 15 mm in diameter and around 5 mm in thickness. The high quality of our samples is tested by x-ray diffraction, and later confirmed by our magnetization and specific-heat measurements. No β phase and other impurities such as Cr_2O_3 were found. The details about the sample preparation by SPS will be reported elsewhere.

The magnetic properties of our samples were measured using a SQUID VSM magnetometer (Quantum Design Inc.). The measurements of specific heat were carried out using a standard thermal relaxation calorimetric method in a commercial Physical Property Measurement System (PPMS, Quantum Design Inc.).

For dielectric measurements, the highly dense pellets of α-MCr_2O_4 prepared by SPS were cut into a rectangle plate first and then polished to a thin sheet with thickness of 0.1–0.3 mm. We use silver paint attached to both sides as electrodes to form a parallel-plate capacitor. The samples are glued on the cryogenic stage of our homemade probe, and connected to a high-precision capacitance meter via low-loss coaxial cables. The main sources of error such as residual impedance in the whole circuit have been carefully compensated.

The electric polarization (P) is obtained from the integration of the corresponding pyroelectric current. We first polarize the specimens with a static electric field of 600–1200 kV/m during the cooling process, then remove the electric field and short circuit the sample at low temperature for about one hour to remove the possible stray charge carriers. The pyroelectric current was measured during the warming process at different heating rates (1–4 K/min).

Aside from the bulk samples prepared by SPS, we also try to grow the single crystals using a high-temperature optical floating zone furnace (FZ-T-12000-X-VPO, Crystal Systems Corp. Japan), which is equipped with four elliptical mirrors and four 3-kW Xenon lamps. At the moment, we can only successfully grow large crystals of α-$SrCr_2O_4$. The shiny flakelike crystals with large area (usually exceeding 4 mm^2) can be easily cleaved from the boule, and they are highly a-axis oriented. Only the dielectric properties along the a axis can be measured since these flake-like crystals are very thin (less than 0.5 mm). X-ray phi-scan measurements on a four-circle diffractometer reveal highly 60°-twinning structures in these crystals since the in-bc-plane orthogonal structure in α-$SrCr_2O_4$ is very close to an ideal hexagonal lattice. Therefore, the in-plane anisotropic physical properties (along the b or c axes) can not be distinguished at present. The crystal growth, together with the corresponding characterization of its structural and physical properties, will be reported in detail elsewhere.

III. EXPERIMENTAL RESULTS

A. α-$SrCr_2O_4$

First, we present the results on α-$SrCr_2O_4$, including its magnetic susceptibility, specific heat, and, especially, dielectric and ferroelectric properties of the bulk samples. Some results on crystal samples are also presented.

1. Magnetic properties

We measured the magnetic susceptibility (χ) of bulk α-$SrCr_2O_4$ samples in several magnetic fields. The $\chi(T)$ curves measured in both the zero-field-cooling (ZFC) and the field-cooling (FC) processes almost merge together. The linear behavior in the field-dependent magnetization (M-H curve, not shown here) is observed up to $H = 7$ T (the limit of our SQUID VSM magnetometer) at several different temperatures below and above the magnetic transition temperature, indicating that the basic magnetic structure in α-$SrCr_2O_4$ holds robust even in a strong field and no possible metamagnetic transition such as spin flop or flip occurs.

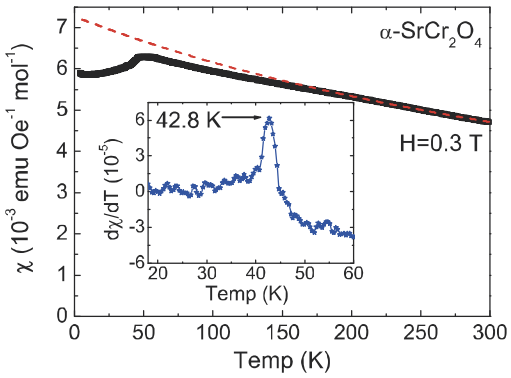

FIG. 2. (Color online) The temperature dependence of magnetic susceptibility (χ). The red dashed line is the Curie-Weiss fit. The corresponding temperature derivative ($d\chi/dT$) is shown in the inset.

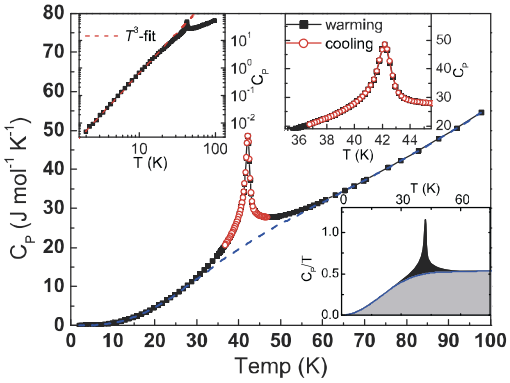

FIG. 3. (Color online) Temperature dependence of the specific heat $C_p(T)$ for α-$SrCr_2O_4$. The main frame shows the data measured in warming (solid square) and cooling processes (open circles). The dashed blue line represents the background to be subtracted to estimate the change in entropy by the anomaly peak around T_N. The corresponding $C_p(T)/T$ curve is shown in the bottom right inset. The upper right inset focuses $C_p(T)$ in the region around the magnetic transition. The overall $C_p(T)$ is also plotted on the log-log scale in the upper left inset, with a Debye-type T^3 power fit (red dashed line) to the low-temperature part of $C_p(T)$.

The main frame in Fig. 2 shows the overall temperature dependence of magnetic susceptibility measured on a typical bulk sample in $H = 0.3$ T. Upon cooling from room temperature, $\chi(T)$ of α-$SrCr_2O_4$ increases gradually. At low temperature, $\chi(T)$ shows a broad hump with a maximum around 50 K, reflecting a typical characteristic of a fluctuating short-range antiferromagnetic ordering in low-dimensional systems. As temperature decreases further, $\chi(T)$ drops abruptly at about 43 K, indicating the emerging of a long-range antiferromagnetic ordering. For clarification, the corresponding temperature derivative ($d\chi/dT$) is plotted in the inset. The Néel temperature for this antiferromagnetic transition T_N can be accurately determined from the peak in $d\chi(T)/dT$. T_N is about 42.8 K, which is consistent with reported results.[24]

Above T_N, the behavior of $\chi(T)$ does not fit well with the Curie-Weiss formula [$\chi(T) = C/(T - \theta_{CW})$], except in the high-temperature range between 200 and 300 K. The fitted curve (dashed line) is also plotted in Fig. 2. The acquired Curie-Weiss temperature θ_{CW} is $-552(.5)$ K, much larger than T_N. The f value (the quantity defined as θ_{CW}/T_N, an empirical measure of frustration) is relatively large (close to 13), indicating a strong magnetical frustration in α-$SrCr_2O_4$. The effective magnetic moment (calculated from the fitted C parameter) is $\mu_{eff} = 4.0(2)\mu_B$, consistent with the previous results.[24] However, the expected moment value for the paramagnetic $S = 3/2$ Cr^{3+} ion is $3.87\mu_B$. The difference may be attributed to the narrow temperature range over which the Curie-Weiss fitting was carried out. The fit to the high temperature $\chi(T)$ (T changes from 300 to 1000 K) in α-$CaCr_2O_4$ has given a quite close value to the expected moment.[23] Therefore, for a better Curie-Weiss fitting, the measurement of $\chi(T)$ well above room temperature is needed in our further work.

2. *Heat-capacity measurements*

The further evidence of the long-range antiferromagnetic ordering in α-$SrCr_2O_4$ comes from the measurement of specific heat (C_p). The $C_p(T)$ shows a sharp λ-shaped anomaly at T_N (see Fig. 3). The overall behavior agrees well with the published data on the α-$SrCr_2O_4$ bulk sample, which was prepared via a conventional method by Dutton *et al.*[24] It is noticeable that the weak anomalous feature at 35 K reported in their work (Fig. 3 in Ref. 24) is not observed in our data, indicating that the 35-K anomaly may come from some unknown impurities in their sample or a possible experimental artifact.

The total specific heat consists of two main contributions, one from lattice vibrations (phonons) and the other from magnetic excitations (magnons), i.e., $C_p \approx C_{phonon} + C_{magnon}$. For magnetic systems of transition metal with nontrivial exchange, these two contributions are usually comparable, especially in low temperature, as summarized by Gopal.[28] As shown in the upper left inset in Fig. 3, A simple T^3 power fit (thin solid line) agrees well with the experimental data below 20 K. It is well known that C_{phonon} obeys the Debye T^3 power law at low temperature. Therefore, the magnetic contribution should also obey the similar T^3 law, i.e., $C_{magnon} \propto T^3$. The T^3 powerlike behavior for C_{magnon} confirms the long-range antiferromagnetic ordering in α-$SrCr_2O_4$,[28] and excludes other possibilities of ferromagnetism and ferrimagnetism, which both obey the $T^{3/2}$ law.[28]

At present, it is hard to extract solely the magnetic part in $C_p(T)$ accurately due to the absence of nonmagnetic isostructural analogs to estimate the contribution of the lattice vibration to the total specific heat. To just estimate roughly the entropy removed by the long-range antiferromagnetic ordering, which is signaled by the peak of $C_p(T)$ around T_N, we use the power-series expansion fit to the high-temperature (>60 K) and low-temperature (<25 K) regimes as the background (the blue dashed line shown in Fig. 3). The entropy, obtained from integrating the anomaly part in $C_p(T)/T$ (the dark gray shadow in the bottom inset), is 2.9 J/mol K, only 12.6% of the full magnetic entropy associated with $2R\ln(2S + 1) \approx 23.05$ J/mol K as expected for an $S = 3/2$ spin system. Most of remaining magnetic entropy is considered to be removed by the short-range ordering well above T_N, as usually observed in the low-dimensional frustrated systems.[16]

There is still no consensus yet regarding the order of the magnetic transition in α-MCr$_2$O$_4$.[22–24,26] We further checked whether there exists any hysteresis in specific heat during the heating and cooling cycle around T_N. For bulk α-SrCr$_2$O$_4$, the two sets of data merge well within the limit of our experimental resolution (the details are shown in the upper right inset in Fig. 3). The same results are also observed on other samples with M = Ca, Ba (not shown here). Considering the fact that people did not observe any corresponding structural transition at T_N until now, our results support the nature of second order in this antiferromagnetic transition at T_N.

3. *Bulk dielectric and pyroelectric measurements*

Figure 4(a) shows the raw capacitance data, which is proportional to dielectric constant (ϵ), measured on a typical sample of bulk α-SrCr$_2$O$_4$ in zero field during the warming process. The different testing frequencies (ranging from 30 kHz to 1 MHz) are used to exclude the possible nonintrinsic artifacts. Similar dielectric behaviors have been observed for all the testing frequencies in our measurements.

At high temperature, the dielectric constant for α-SrCr$_2$O$_4$ decreases gradually upon cooling, which is typical for most insulating materials. But, below roughly 100 K, the dielectric constant turns around to become slightly increasing with decreasing temperature. The anomalous increase in $\epsilon(T)$ is likely related to the short-range antiferromagnetic ordering emerging well above T_N via magnetoelectric correlations. It has been observed in other systems such as TeCuO$_3$ that the short-range magnetic correlations affect dielectric properties.[29]

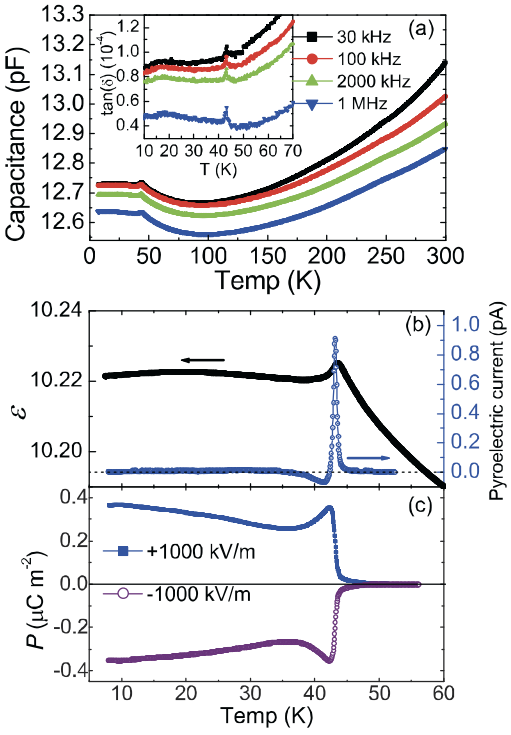

FIG. 4. (Color online) (a) Raw capacitance data of a typical α-SrCr$_2$O$_4$ sample measured at different frequencies in zero field. The corresponding dielectric loss (tanδ) is shown in the inset. (b) Temperature dependence of the dielectric constant (black) measured at a frequency of 100 kHz and pyroelectric current (blue) measured in the warming process after poling with a electric field of 1000 kV/m. The dashed line represents zero pyroelectric current. (c) Electric polarization (P) vs temperature, using both positive (blue) and negative (cyan) poling electric fields.

The most remarkable feature is the small lambdalike dielectric anomaly peaked at the T_N, concurrently with the emerging of a long-range magnetic ordering, which has been observed in the magnetization and heat-capacity measurements. Correspondingly, a very weak peak arises in the correspondingly dielectric loss (tanδ) at the same temperature (shown in the inset), indicating the signature of a weak but corroborative intrinsic ferroelectric transition at T_N.

Aside from adopting different testing frequencies, we have also confirmed the anomalous features in $\epsilon(T)$ by repeating the temperature cycles and on samples of different batches (the same testing procedures were carried out on other samples such as α-phase CaCr$_2$O$_4$ and BaCr$_2$O$_4$, which are discussed later). Therefore, possible extrinsic factors such as trapped interfacial charge carriers and thermal degradation of bulk sample can be excluded. The observed anomalies indicate an intrinsic electric transition at T_N. For convenience, we only use the data measured at 100 kHz in our following discussions.

The weak ferroelectricity in α-SrCr$_2$O$_4$ is further confirmed in our measurements of electric polarization using the pyroelectric method. Figure 4(b) shows the pyroelectric data, along with the corresponding dielectric constant, measured on a typical bulk sample. A quite small (below 1 pA) but very sharp peak emerges as the temperature approaches T_N. The current drops to zero as $T \geqslant T_N$. The P is acquired by integrating the pyroelectric current from above T_N. A clear development of a spontaneous electric polarization P below the magnetic ordering temperature is shown in Fig. 4(c). Below T_N, P can be inverted with the opposite poling electric field, proving its ferroelectric nature. At T = 10 K, P saturates at about 0.36 μC/m^2, a very small value which is several orders smaller than most known multiferroic materials,[6] but of the same order as the published data on isostructural α-CaCr$_2$O$_4$ by Singh *et al.*[26]

Another important feature is from the temperature-dependent pyroelectric current. As temperature increases, a small negative pyroelectric hump arising around 40 K, as a precursor close to the sharp peak just below T_N, as shown in Fig. 4(b). Correspondingly, as temperature decreases from above T_N, P first goes up rapidly from zero to a maximum just below T_N, then P decreases as the result of the emerging negative pyroelectric current. P continues to decrease to a minimum at about 37 K, at which the negative pyroelectric current vanishes. Upon further cooling, P increases very slowly and saturates at lowest temperature. The decreasing in P on cooling in a narrow temperature range (between 37 and 42 K) is rarely observed in conventional ferroelectric materials. It is noted that such an anomaly has been observed on the α-CaCr$_2$O$_4$ samples by Singh *et al.* without giving the corresponding explanation.[26] The possible artifacts such as interfacial trapped carriers have been carefully excluded by reversing poling electric field and adopting different heating rate in our measurements. Jodlauk *et al.* have also observed the similar negative pyroelectric currents on some multiferroic pyroxenes.[30] Although its origin

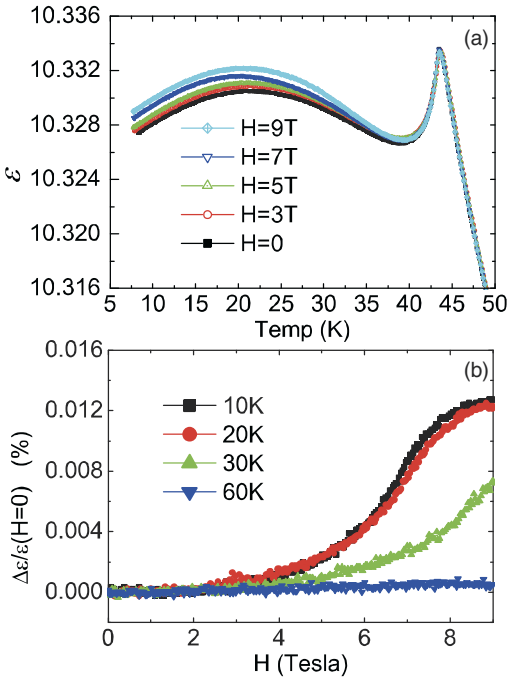

FIG. 5. (Color online) (a) Temperature dependence of dielectric constant (ϵ) for α-$SrCr_2O_4$ in different applied magnetic fields ($H = 0$–9 T). (b) Magnetic field dependence of ϵ at several temperatures above ($T = 60$ K) and below ($T = 10, 20, 30$ K) the magnetic transition temperature.

is not yet clear, the observed anomaly is unlikely attributed to ferroelectricity. One possible explanation is the existence of the strong antiferroelectric correlation between the CrO_2 layers, which will be discussed later.

4. *Magnetoelectric coupling in bulk α-$SrCr_2O_4$*

We further investigated the magnetoelectric coupling effect in α-$SrCr_2O_4$ in magnetic field up to 9 T, which is parallel with the plate-like sample (i.e., H⊥E configuration). We also tested the H||E measuring configuration in our experiments. No noticeable difference was observed since the intrinsic anisotropy is possibly canceled out in our polycrystalline samples.

The $\epsilon(T)$ under different fields ($H = 0$–9 T) is measured [see Fig. 5(a)]. No noticeable temperature shift of the antiferromagnetic transition (deduced from the peak of dielectric anomaly) is observed, confirming the robustness of the helimagnetic structure in α-$SrCr_2O_4$. At high temperatures, $\epsilon(T)$ is almost not affected by H. Below T_N, $\epsilon(T)$ increases quite slightly upon increasing H. The effect on $\epsilon(T)$ by H is vanishing small (an order of 10^{-5}) and it develops slightly with further cooling. We also measured $P(T)$ under different fields (not shown here), and the difference is negligible within the experimental resolution of our setup.

To quantify this magnetoelectric coupling effect more precisely, we measured the magnetoelectric coefficients {MC, defined as $[\epsilon(H) - \epsilon(H = 0)]/\epsilon(H = 0)$} at several temperature points above and below T_N [see Fig. 5(b)]. Above T_N, MC is almost zero, suggesting the magnetoelectric coupling in α-$SrCr_2O_4$ is associated only with the long-range magnetic

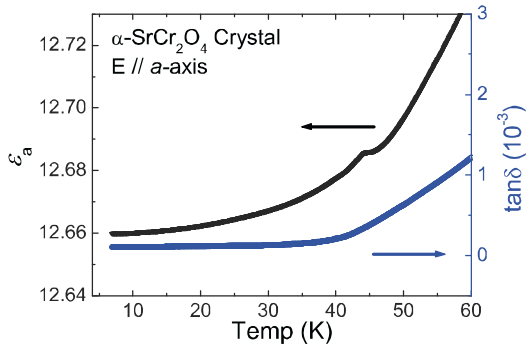

FIG. 6. (Color online) (a) Temperature dependence of a-axis dielectric constant (ϵ_a) and corresponding loss (tanδ) measured on a flakelike α-$SrCr_2O_4$ crystal sample grown by optical floating zone method. The testing electric field E is along the a axis.

ordering below T_N. At $T < T_N$, MC is positive and increases with decreasing temperature. In addition, the corresponding magnitude is very small, only reaching 10^{-4} at the highest field $H = 9$ T, much smaller than most of the known multiferroic materials.[6]

At each temperature point below T_N, MC increases with increasing H, approximately proportional to the square of the field, except the saturating part in the high-field region($H \geqslant 8$ T). This quasiquadratic magnetoelectric effect is consistent with the empirical analysis based on the analysis of the Landau free energy and symmetry consideration by Chapon and Singh *et al.*[22,26]

5. *Results on crystal samples of α-$SrCr_2O_4$*

As aforementioned, our flake-like crystal samples of α-$SrCr_2O_4$ are highly a-axis oriented, with quasi-60° twinning in the bc plane. Therefore, only the dielectric constant and electric polarization along the a axis (ϵ_a and P_a) can be measured at present. In low temperature, the corresponding magnetic susceptibilities in H⊥a and H||a have been measured (not shown), and both behave very similar as the bulk sample, which is consistent with the published data on the isostructural crystals of α-$CaCr_2O_4$ by Toth *et al.*[23]

As shown in Fig. 6, in zero field, $\epsilon_a(T)$ decreases gradually on cooling. Around T_N, only a very weak hump is observed. This weak anomaly in $\epsilon_a(T)$ is associated with the multiferroic transition, which has been observed on bulk samples. No anomaly at T_N can be visible in the corresponding dielectric loss. We also measured $\epsilon_a(T)$ under different H, the influence in $\epsilon_a(T)$ by H is negligible. In our pyroelectric measurements, no net electric polarization (P_a) is observed within our experimental resolution, which strongly contrasts against the results on the bulk samples. This result suggests the absence of ferroelectricity along the a axis in α-$SrCr_2O_4$. Thus, the intrinsic ferroelectric polarization, arising from the magnetic ordering in α-$SrCr_2O_4$, must lie in the bc plane.

At present, our crystal samples and the experimental setup do not allow us to determine the exact direction of in-bc-plane polarization. According to the analysis of magnetic symmetry,[14] the proper-screw-type spin ordering, which emerges below T_N, breaks the spatial inversion and mirror operation, and makes the only allowed $2'$ operation

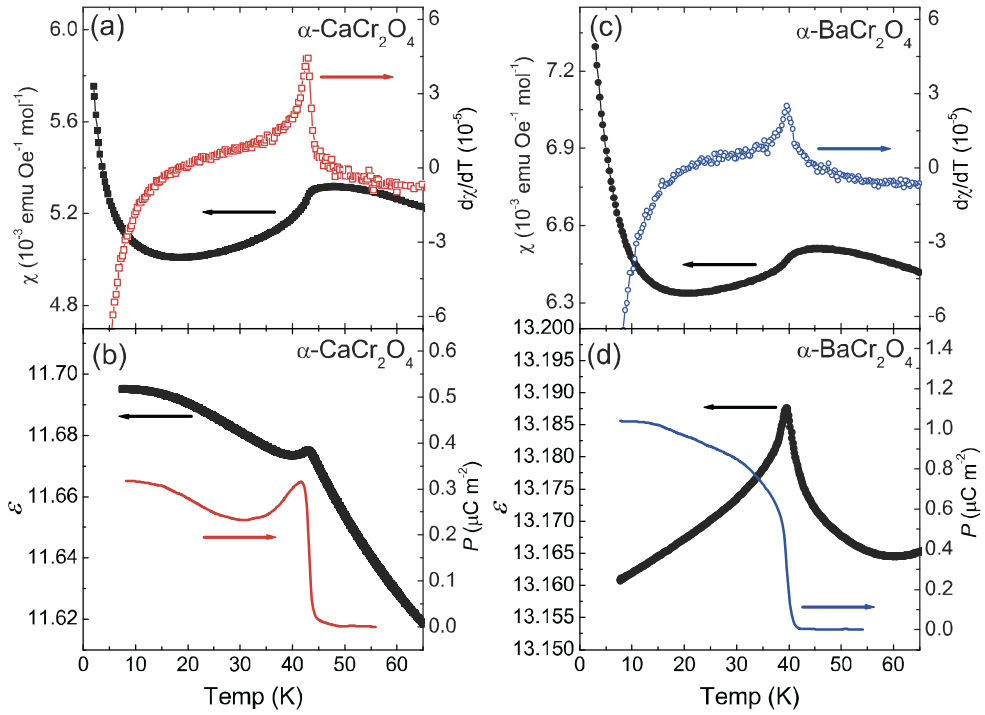

FIG. 7. (Color online) Temperature dependence of the magnetic susceptibility (χ), the corresponding $d\chi/dT$, the dielectric constant (ϵ), and the electric polarization (P) of α-$CaCr_2O_4$ (a), (b) and α-$BaCr_2O_4$ (c), (d).

axis along the the magnetic modulation vector (b axis in α-$SrCr_2O_4$). So, the polar order should appear in this direction. The growth of large untwinned single crystals is necessary in our further studies on its anisotropic properties.

B. α-phase $CaCr_2O_4$ and $BaCr_2O_4$

The other two members in the family of α-MCr_2O_4 with different alkaline-earth elements (M = Ca, Ba) have also been synthesized by the SPS method. On the whole, their physical properties are quite similar to those of α-$SrCr_2O_4$.

Figures 7(a) and 7(c) show $\chi(T)$ and the corresponding temperature derivatives ($d\chi/dT$) for bulk samples of α-phase $CaCr_2O_4$ and $BaCr_2O_4$, respectively. The antiferromagnetic humps in $\chi(T)$ are clearly observed on both compounds, very similar to that of α-$SrCr_2O_4$. The neutron diffraction measurements on the powder and single-crystal samples of α-$CaCr_2O_4$ (Refs. 22 and 23) have revealed a long-range incommensurate proper-screw-type helimagnetic ground state, which is almost identical to that observed in α-$SrCr_2O_4$.[24] An analogous helical spin picture in α-$BaCr_2O_4$ was just proposed based on the recent neutron powder diffraction by Hardy *et al.*[25] The high similarity of magnetic structures in the α-MCr_2O_4 family accounts for their analogous magnetic properties, which comes from the basal structure of the quasi-2D triangular CrO_2 layers.

The clear kink in $\chi(T)$ labels the emerging of a long-range magnetic ordering. The corresponding T_N is determined accurately according to the sharp peak in $d\chi/dT$. T_N of α-$CaCr_2O_4$ is 43.0 K, very close to that of α-$SrCr_2O_4$ (42.8 K). However, for α-$BaCr_2O_4$, T_N drops to 39.5 K, a few Kelvins lower than the other two members. The difference can be easily understood, considering the much larger interlayer spacing in α-$BaCr_2O_4$ (6.14 Å) than the other two members (5.53 Å for α-$SrCr_2O_4$ and 5.82 Å for α-$CaCr_2O_4$). The smaller separation between the triangular CrO_2 layers can enhance the interlayer interactions, which helps to stabilize the long-range ordering in the frustrated spin systems.

As shown in Figs. 7(b) and 7(d), such as α-$SrCr_2O_4$, the $\epsilon(T)$s of both α-$CaCr_2O_4$ and α-$BaCr_2O_4$ show anomalous peaks with their corresponding maxima exactly located at their T_N (43.0 and 39.5 K, respectively), coinciding well with the emerging of the long-range magnetic ordering. The corresponding difference between them is also considerable. The $\epsilon(T)$ of α-$CaCr_2O_4$ exhibits a very weak peak at T_N, followed by a slow increase on further cooling, which behaves quite similar with α-$SrCr_2O_4$. As cooled from above T_N, the $P(T)$ arises sharply just below T_N, from zero to a maximum, then followed by a drop until 30 K due to the emergent negative pyroelectric currents (not shown) as observed in α-$SrCr_2O_4$ [shown in Fig. 4(b)]. The behavior of $P(T)$ resembles that of α-$SrCr_2O_4$ closely. The P at 10 K is 0.31 $\mu C/m^2$, slightly lower than α-$SrCr_2O_4$.

On the other hand, around T_N(=39.5 K), the peak in $\epsilon(T)$ of α-$BaCr_2O_4$ is much more pronounced than the other two analogs. The $\epsilon(T)$ decreases monotonously with further cooling below T_N. The salient peak indicates a stronger ferroelectric transition. No negative pyroelectric current is observed on α-$BaCaCr_2O_4$ samples below T_N. Correspondingly, $P(T)$ increases monotonously upon cooling as $T < T_N$. $P(T = 10\ \text{K})$ reaches to 1 $\mu C/m^2$, about two times larger than the Sr or Ca analogs.

As for the magnetoelectric effect in α-$CaCr_2O_4$ and α-$BaCr_2O_4$, both compounds exhibit a very weak

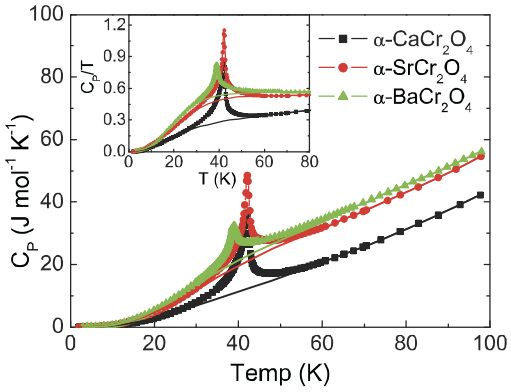

FIG. 8. (Color online) Temperature dependence of the specific heat measured for three bulk samples of α-phase $CaCr_2O_4$, $SrCr_2O_4$, and $BaCr_2O_4$. The dashed lines are the corresponding backgrounds to be subtracted to estimate the change of entropy by the specific-heat anomalies, respectively. The corresponding $C_p(T)/T$ is plotted in the inset.

magnetoelectric coupling below T_N as α-$SrCr_2O_4$ (not shown). The MC values increase quasiquadratically with respect to H, achieving the order of only 10^{-4} even at the highest $H = 9$ T, similar as in α-$SrCr_2O_4$.

For a comprehensive understanding of the long-range magnetic ordering in the α-MCr_2O_4 family, we plot all the specific-heat data for all these three member compounds in Fig. 8. The clear λ-shaped anomaly peak is visible for each sample. There are no temperature shifts of the peak in $C_p(T)$ during the warming and cooling measuring process, which suggests the nature of second order in the magnetic transitions in this family.

To estimate the entropy removed by the long-range magnetic ordering which was signaled by the peak of $C_p(T)$ anomaly around T_N, we use the same procedure as described earlier. The baseline for background subtraction (shown as dashed lines in Fig. 8) shifts vertically as M changes from the lightest element (Ca) to the heaviest Ba atom, consistent with the known Debye model for the specific heat of phonons. The different M atoms contribute the lattice specific heat since Debye temperature $\theta_D \propto 1/\sqrt{W}$ where W is the molecular weight.

The calculated change in entropy for α-phase $SrCr_2O_4$, $CaCr_2O_4$, and $BaCr_2O_4$ is 3.6, 2.9, 2.0 J/mol K, respectively, which is equivalent to 15.6%, 12.6%, 8.5% of the total magnetic entropy, respectively. Apparently, most of the missing entropy is removed by low-dimensional short-range ordering well above T_N. The change in entropy decreases as the radius of interlayer nonmagnetic M ions increases. The increase in the spacing between CrO_2 layers can weaken the interlayer interaction, and drive the system closer to the ideal low dimensionality and therefore the short-range ordering above T_N becomes more dominant.

IV. DISCUSSIONS

The strong geometrically magnetic frustration and low dimensionality dominate the physics in the α-MCr_2O_4 family. The previous neutron diffraction experiments have revealed that there exists a quasi-120° proper-screw-type helical spin structure with the magnetic propagation vector along the b axis emerging below T_N. This quasi-120° spin picture is energetically favorite, consistent with the theory for 2D triangular lattice, which leads to the overall similar low-temperature magnetic properties in this family.

The similar properties of magnetization, specific heat, dielectric constant, and ferroelectric polarization in these three members have been observed in our experiments. The very weak multiferroicity (compared with many known multiferroic materials[6]) is confirmed below T_N, concomitant with the proper-screw-type spin ordering as $T < T_N$. In order to better understand our observations, we analyzed our results in comparison with the existing theoretical models on the microscopic mechanism of multiferroicity. All the spins at Cr^{3+} sites are equivalent ($S = 3/2$). The macroscopic net-exchange striction in helical magnetic structure averages to zero. So, the magnetostriction can not give net electric polarization. On the other hand, according to the inverse DM mechanism or the spin-current model, this proper-screw-type helical spin can not induce any microscopic electric polarization.

A more plausible candidate, as proposed by Arima and Jia *et al.*,[14,15] is the d-p hybridization modified by the spin-orbital interactions in partially filled t_{2g} systems, which can induce the microscopic electric polarization along the bond direction. This kind of local polarization can be expressed as $\mathbf{P}_{ij} \propto (\boldsymbol{S}_i\ \hat{\mathbf{e}}_{ij})\boldsymbol{S}_i - (\boldsymbol{S}_j\ \hat{\mathbf{e}}_{ij})\boldsymbol{S}_j$, where $\hat{\mathbf{e}}_{ij}$ is the unit vector connecting the neighboring sites i and j. Although this term is oscillating and usually cancels out in zero in most crystals, in certain geometries such as 2D triangular systems with inversion-symmetry-breaking proper-screw-type helimagnetism, the net components along the modulation vector have been shown to be nonzero.[14] This is the case in the α-MCr_2O_4 family with proper-screw-type helimagnetism modulated along the b axis. Therefore, the electric polarization is expected along the b axis, which is also consistent with the proposed b-axis polar order based on the symmetry analysis. In our measurements on crystal samples of α-$SrCr_2O_4$, no ferroelectricity along the a axis can be observed, supporting the above theoretical analysis.

The effect of interlayer interaction has not be considered in Arima's theory. So far, we have observed that the multiferroicity in α-MCr_2O_4 is enhanced as M changes from Ca to Ba with increasing separation between CrO_2 layers. The negative hump of pyroelectric currents is observed in α-$SrCr_2O_4$ and α-$CaCr_2O_4$ with small interlayer spacings, which may arise from the antiferroelectric correlations between the CrO_2 layers, and lead to the decrease of $P(T)$ on cooling below T_N. But, this behavior no longer exists in α-$BaCr_2O_4$, which has larger interlayer spacing than the other two members in this family. The interlayer exchange interaction in the α-MCr_2O_4 family accounts for this weak antiferroelectric interlayer coupling. The similar interlayer antiferroelectric coupling has also been discussed in some $ACrO_2$ (A is alkali metal) systems in detail by Seki *et al.*[13] Although the interlayer interaction stabilizes the long-range ordering and help to achieve higher T_N, it also favors the antiferroelectric coupling between triangular layers and greatly suppresses the total macroscopic polarization. The stronger multiferroicity seems to favor the more ideal low dimensionality.

V. CONCLUSION

In this paper, the quasi-2D geometrically frustrated triangular magnetic system α-MCr_2O_4 (M = Ca, Sr, Ba) was systematically investigated, and the multiferroicity has been confirmed concomitant with the long-range magnetic ordering below T_N in this family. The possible microscopic mechanism of this spin-driven ferroelectricity is attributed to the Arima model for the proper screw type of helical magnetic ordering in a triangular antiferromagnetic lattice. The evolution of multiferroic properties with the increasing separation of the stacking CrO_2 layers is also discussed. Our present studies provide valuable information for the further search of new multiferroics in geometrically frustrated magnetic systems.

ACKNOWLEDGMENTS

We wish to acknowledge M. J. Wang, W. L. Lee, and C. C. Li for their technical support and helpful discussions. We also acknowledge the financial support from Academia Sinica and the National Science Council of Taiwan.

*mkwu@phys.sinica.edu.tw

[1] T. Kimura, T. Goto, H. Shintani, K. Ishizaka, T. Arima, and Y. Tokura, Nature (London) **426**, 55 (2003).
[2] N. Hur, S. Park, P. A. Sharma, J. S. Ahn, S. Guha, and S.-W. Cheong, Nature (London) **429**, 392 (2004).
[3] M. Fiebig, J. Phys. D: Appl. Phys. **38**, R123 (2005).
[4] S.-W. Cheong and M. Mostovoy, Nat. Mater. **6**, 13 (2007).
[5] R. Ramesh and N. A. Spaldin, Nat. Mater. **6**, 21 (2007).
[6] K. F. Wang, J.-M. Liu, and Z. F. Ren, Adv. Phys. **58**, 321 (2009).
[7] Y. J. Choi, H. T. Yi, S. Lee, Q. Huang, V. Kiryukhin, and S.-W. Cheong, Phys. Rev. Lett. **100**, 047601 (2008).
[8] I. A. Sergienko and E. Dagotto, Phys. Rev. B **73**, 094434 (2006).
[9] H. Katsura, N. Nagaosa, and A. V. Balatsky, Phys. Rev. Lett. **95**, 057205 (2005).
[10] M. Mostovoy, Phys. Rev. Lett. **96**, 067601 (2006).
[11] S. Park, Y. J. Choi, C. L. Zhang, and S.-W. Cheong, Phys. Rev. Lett. **98**, 057601 (2007).
[12] T. Kimura, J. C. Lashley, and A. P. Ramirez, Phys. Rev. B **73**, 220401 (2006).
[13] S. Seki, Y. Onose, and Y. Tokura, Phys. Rev. Lett. **101**, 067204 (2008).
[14] T. Arima, J. Phys. Soc. Jpn. **76**, 073702 (2007).
[15] C. Jia, S. Onoda, N. Nagaosa, and J. H. Han, Phys. Rev. B **76**, 144424 (2007).
[16] A. P. Ramirez, Annu. Rev. Mater. Sci. **24**, 453 (1994).
[17] M. F. Collins and O. A. Petrenko, Can. J. Phys. **75**, 605 (1997).
[18] K. Motida and S. Miyahara, J. Phys. Soc. Jpn. **28**, 1188 (1970).
[19] H. Pausch and H. K. Mller-Buschbaum, Z. Anorg. Allg. Chem. **405**, 113 (1974).
[20] H. Pausch and H. K. Mller-Buschbaum, Z. Anorg. Allg. Chem. **405**, 1 (1974).
[21] E. Cuno and H. K. Mller-Buschbaum, Z. Anorg. Allg. Chem. **564**, 26 (1988).
[22] L. C. Chapon, P. Manuel, F. Damay, P. Toledano, V. Hardy, and C. Martin, Phys. Rev. B **83**, 024409 (2011).
[23] S. Toth, B. Lake, S. A. J. Kimber, O. Pieper, M. Reehuis, A. T. M. N. Islam, O. Zaharko, C. Ritter, A. H. Hill, H. Ryll, K. Kiefer, D. N. Argyriou, and A. J. Williams, Phys. Rev. B **84**, 054452 (2011).
[24] S. E. Dutton, E. Climent-Pascual, P. W. Stephens, J. P. Hodges, A. Huq, C. L. Broholm, and R. J. Cava, J. Phys.: Condens. Matter **23**, 246005 (2011).
[25] V. Hardy *et al.* (unpublished).
[26] K. Singh, C. Simon, and P. Toledano, Phys. Rev. B **84**, 064129 (2011).
[27] F. Damay, C. Martin, V. Hardy, A. Maignan, G. Andre, K. Knight, S. R. Giblin, and L. C. Chapon, Phys. Rev. B **81**, 214405 (2010).
[28] E. S. R. Gopal, *Specific Heat at Low Temperatures* (Plenum, New York, 1966).
[29] G. Lawes, A. P. Ramirez, C. M. Varma, and M. A. Subramanian, Phys. Rev. Lett. **91**, 257208 (2003).
[30] S. Jodlauk, P. Becker, J. A. Mydosh, D. I. Khomskii, T. Lorenz, S. V. Streltsov, D. C. Hezel, and L. Bohaty, J. Phys.: Condens. Matter **19**, 432201 (2007).